Frustration and anomalous behavior in the Bell-Lavis model of liquid water

Marco Aurélio Alves Barbosa and Vera Bohomoletz Henriques*
Instituto de Física, Universidade de São Paulo, Caixa Postal 66318, 05315970 São Paulo, São Paulo, Brazil
(Received 18 January 2008; published 19 May 2008)

We have reconsidered the Bell-Lavis model of liquid water and investigated its relation to its isotropic version, the antiferromagnetic Blume-Emery-Griffiths model on the triangular lattice. Our study was carried out by means of an exact solution on the sequential Husimi cactus. We show that the ground states of both models share the same topology and that fluid phases (gas and low- and high-density liquids) can be mapped onto magnetic phases (paramagnetic, antiferromagnetic, and dense paramagnetic, respectively). Both models present liquid-liquid coexistence and several thermodynamic anomalies. This result suggests that anisotropy introduced through orientational variables play no specific role in producing the density anomaly, in agreement with a similar conclusion discussed previously following results for continuous soft core models. We propose that the presence of liquid anomalies may be related to energetic frustration, a feature common to both models.

DOI: 10.1103/PhysRevE.77.051204 PACS number(s): 61.20.Gy, 65.20.−w

I. INTRODUCTION

Water is one of the most intriguing fluids in nature due to its peculiar properties, relative abundance, and relevance for life. In the liquid phase, several of its properties are recognized as anomalous, since they are unusual in liquids with the same molecular size as H_2O. Among its anomalous features, the best known is probably the increase in density with temperature that happens from the melting point up to 4 °C, at atmospheric pressures. The density anomaly exists in a large region of the pressure-temperature phase diagram and forms a line of temperatures of maximum density (TMD), which has negative inclination and enters the supercooled metastable regime above 40 MPa [1]. Other important anomalous quantities are the basic thermodynamic derivatives: heat capacity C_P, thermal expansion α_P, and isothermal compressibility k_T, whose magnitudes increase as the temperature is lowered toward the supercooled regime, at lower pressures [2–4].

Different thermodynamic scenarios have competed to describe the presence of anomalies in liquid water. Two of them, the stability limit conjecture [5] and the second-critical-point hypothesis [6], assign the origin of these phenomena to thermodynamic instabilities in the supercooled regime. These would be due to the retracing of the gas-liquid spinodal to positive temperature, in the former case, or to a second critical point, related to the end of a liquid-liquid phase transition at high pressures, in the latter case. The second-critical-point hypothesis has received a lot of attention lately because liquid-liquid phase transitions, which were originally found in simulations of realistic models of water [6], were also found in simulations of SiO_2 [7] and in high-temperature x-ray diffraction experiments of phosphorus [8,9]. In addition to these results, there is some experimental evidence of a phase transition between two amorphous phases of water [10,11] as well as for other substances [12], which might possibly be related to the low-temperature continuation of the liquid-liquid phase transition. The third possibility is the singularity-free scenario [13,14], which is based on a set of thermodynamical equations connecting the increase in magnitude of k_T, C_P, and α_P to the presence of a TMD line of a negative slope in the pressure vs temperature plane.

Despite the lack of consensus on the thermodynamic description behind liquid anomalies, it is widely accepted that the hydrogen bond is responsible for them in water. At ambient pressure, hydrogen bonds create a fully bonded, tetrahedral structure in ice Ih, which is less dense than the liquid phase. Since the latent heat of fusion is not enough to break all bonds, these structures are partially preserved in the liquid. At the same time, the existence of a "normal liquid" structure, which is less bonded and more dense than the former structure, creates a free energy competition between different liquids that results in a density anomaly [15].

Different kinds of interactions have been used to implement the above description in statistical fluid models. Many reproduce the density anomaly and other waterlike properties. Models could be grouped into two main categories: isotropic and orientational. In both groups, continuous as well as lattice models, more tractable in analytical calculations, and easier to simulate, have been presented.

Core-softened continuous and lattice models, and lattice-volume-dependent Potts state models belong in the first group. In the so-called core-softened models it is considered that the relevant feature is the presence of two characteristic lengths: the range of the usual attractive interaction and the range of a soft repulsive interaction, in addition to the hard core [16–25]. This additional interaction would be responsible for the competition between fluids of different densities. A few lattice versions of the core-softened models were implemented with nearest-neighbor and next-nearest-neighbor interactions in one (1D) [26] and two dimensions (2D) [27]. The core-softened models may present density and other anomalies and/or liquid-liquid coexistence, depending on the form of the repulsive soft core and on the presence of an attractive interaction. A different lattice statistical model was presented by Sastry and collaborators: particle states were represented by Potts variables with isotropic bonding, coupled to an *ad hoc* variation of molecular volume

*vera@if.usp.br

 ©2008 The American Physical Society

[13,14]. The latter was used as an example of the singularity-free scenario.

A second group of models emphasizes the orientational character of the hydrogen bond interactions, which for a long time have been accepted as responsible for water anomalies. In the 2D Mercedez-Benz model [28] water molecules are represented by particles with three bonding arms, with no distinction of donors or acceptors, in order to mimic hydrogen bonds. Water thermodynamic and solvation anomalies and also liquid-liquid transitions may be present, under different approaches [29–32]. A lattice version of the Mercedez-Benz model was an early proposal of Bell and Lavis [33], which was investigated in several papers [34–36]. An orientational 3D lattice gas model which allowed for a distinction between donor and acceptor hydrogen bond states was investigated by Roberts and Debenedetti [37,38]. A simpler 2D orientational lattice gas was proposed more recently [39–41]. All these models were shown to exhibit a density anomaly and liquid polymorphism.

In the case of the lattice models, isotropic or orientational, several *ad hoc* features were added, in order to mimic different physical microscopic aspects. In some cases, the denser liquid states are energetically destabilized with a weakening factor that lowers bond strength whenever another molecule comes closer to bonding molecules [37,42–45] or, equivalently, a slightly repulsive *van der Waals* interaction [39,41,46]. In other cases, an additional number of q nonbonding states is assigned to each water molecule, in order to force an entropy increase in the unbonded and disordered liquid [13,14,37,44,45,47]. As mentioned previously, there are also cases in which particle states typical of low temperatures are associated with lower local density [13,14]. In some studies, several of the above structural and energetic elements are present simultaneously.

Despite the fact that most of the mentioned models display some features of liquid water, it is still not possible to ascertain the relevant microscopic aspects that lead to a density anomaly.

In the present study we give a further step in the direction of looking for minimum requirements for a water model. We give a detailed analysis of the properties of the Bell-Lavis model, the simplest known lattice model for a bonding fluid, and compare them to those of its isotropic version, a frustrated antiferromagnet.

The Bell-Lavis (BL) model was proposed almost 40 years ago. It can be interpreted as a triangular lattice version of the Mercedez-Benz model [29]. In the original paper [33], the properties of the BL model were calculated on a triangle, named by the authors as an approximation with short-range order, and it was shown to present a density anomaly. Later, the first approach was improved with the use of three sublattices, named as an approximation with long-range order. Under this approximation, a new phase emerged: a bonded, low-density phase, which the authors identified as solid [34]. The discovery of the new phase led to the conclusion that the liquid density anomaly was in a metastable region, where the solid was stable. Subsequently, an explicit form for the gas-liquid coexistence line, in stable and metastable regimes, was calculated using a symmetry transformation, in the context of the first-order approximation with short-range order. It was then possible to derive analytical expressions for the thermodynamic response functions, which presented behavior similar to that of water [48], with numerically reasonable ratios, for both the temperatures of minimum isothermal compressibility and of maximum density, to the gas-liquid critical temperature [48]. These findings represented interesting features of the model, despite the metastability of the liquid phase. A real space renormalization group [35,36] study was also undertaken, and indicated that the solid-liquid transition was critical, as well as that the TMD occurred in the solid phase, in contradiction with the previous results.

In this paper we reconsider the BL model, through an analysis of the model's ground state and phase diagrams, and try to understand which features are relevant for the appearance of a density anomaly, by considering a simpler version of its Hamiltonian. To achieve this goal, we have chosen to study the isotropic version of the BL Hamiltonian, which is equivalent to the antiferromagnet Blume-Emery-Griffiths (BEG) model on the triangular lattice [49], and to compare the properties of both models using equivalent parameters. We found similarities between the two models' properties, particularly concerning the ground state and the density anomaly.

The thermodynamic properties have been obtained on the Bethe lattice [50], using the recursive approach in a sequentially constructed Husimi cactus [51]. This methodology is appropriate for the study of systems with energetic frustration, as has been discussed elsewhere [51,52], and becomes equivalent to Bell's long-range order approximation [34], in which three sublattices are considered.

We have abandoned the interpretation of the less dense and bonded phase as solid. Such an interpretation requires that the system remain liquid at very high pressures, at low temperatures, which does not seem physically reasonable. We have therefore chosen to name the two phases as liquid, denoting the less dense and bonded phase as *low-density liquid* (LDL), and the disordered liquid as *high-density liquid* (HDL). The liquid-liquid transition could become a transition between two amorphous states, at low temperatures. However, the distinction between the amorphous solid and liquid states is based on viscosity [53] and, so far, there are no studies on diffusion for the BL model.

This paper is organized as follows. In Sec. II the Bell-Lavis model is presented, its Hamiltonian is built using Potts and spin representations, and a comparison is made with the antiferromagnetic Blume-Emery-Griffiths model. In Sec. III the recursive approach to the Husimi cactus is introduced and the description of a frustrated spin-1 system is given [51]. An expression for the grand potential and the mean value of some relevant quantities in the interior of the Husimi cactus are presented, in the same section. The thermodynamics and the liquid structure of both models are analyzed in Sec. IV and concluding remarks are left for the last section.

II. THE BELL-LAVIS MODEL: AN ANISOTROPIC ANTIFERROMAGNETIC BEG MODEL

The Bell-Lavis model is defined on a triangular lattice whose vertices can be either occupied by a molecule, or

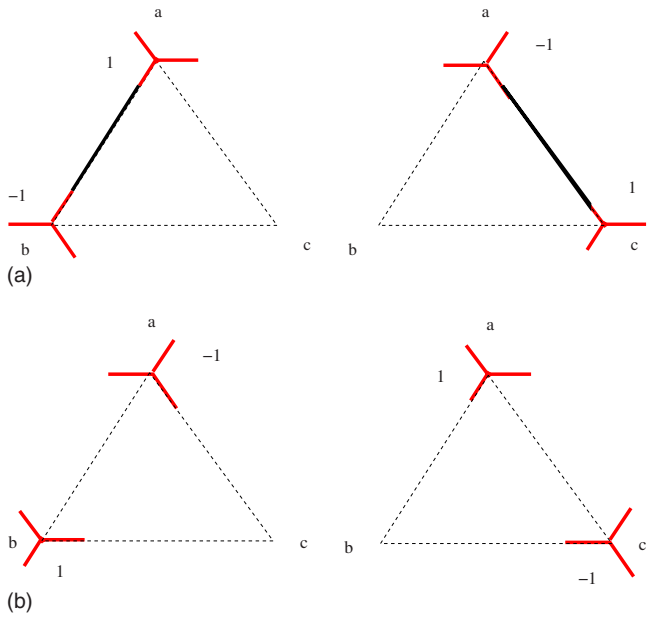

FIG. 1. (Color online) Interactions on the Bell-Lavis water model. (a) Water molecules forming a hydrogen bond with a pair interaction energy of $-(\epsilon_{\mathrm{vdW}}+\epsilon_{\mathrm{hb}})$ and (b) molecules interacting only through van der Waals attraction with a pair interaction energy of $-\epsilon_{\mathrm{vdW}}$.

empty. Each molecule has three bonding arms separated by 120° and two different orientations. The energetics of the model is simple and includes van der Waals interaction and hydrogen bonds between neighboring molecules. Hydrogen bonding depends on specific molecular orientations and happens when the bonding arms of neighboring molecules point to each other. Figure 1 shows examples of (a) bonded and (b) unbonded molecules. The states of a particle are represented through occupational, η_i, and orientational, τ_i^{ij}, variables. η_i indicates the presence or absence of a particle at site i ($\eta_i=1$ or 0, respectively) and τ_i^{ij} stands for the presence or absence of a bonding arm pointing from site i to site j ($\tau_i^{ij}=1$ or 0, respectively). With these definitions, the effective Hamiltonian of the system, in the grand canonical ensemble, can be written as

$$\mathcal{H}_{\mathrm{BL}} = -\sum_{(i,j)} \eta_i \eta_j (\epsilon_{\mathrm{vdW}} + \epsilon_{\mathrm{hb}} \tau_i^{ij} \tau_j^{ji}) - \mu \sum_i \eta_i, \tag{1}$$

where ϵ_{vdW} refers to the strength of the van der Waals interaction, $\epsilon_{\mathrm{hb}}>0$ to the strength of the hydrogen bond interaction, which is attractive by definition, and μ to the chemical potential. The first sum is performed over all pairs (i,j) of nearest neighbors, and the second over all sites i.

Alternatively, this effective Hamiltonian can be written in a spin-1 representation [35]. This will be useful, since it permits one to relate the BL and BEG models naturally. To simplify the calculations, the effective Hamiltonian can be split between the lattice triangles as

$$\mathcal{H}_{\mathrm{BL}} = \frac{1}{2}\sum h_{\mathrm{BL}} = \frac{1}{2}\sum (h_{\mathrm{vdW}} + h_{\mathrm{hb}} + h_{\mu}), \tag{2}$$

where the summation is over all triangles in the lattice and the factor 1/2 avoids double counting of links on adjacent triangles. In Eq. (2) we separate the contributions coming from van der Waals interactions, hydrogen bonds and chemical potential, by defining the terms h_{vdW}, h_{hb}, and h_{μ}. Now, let us assume that the state of each site k in a triangle is represented by a spin S_k which assumes integer values for different particle orientations (see Fig. 1), and 0 for a hole. As will be seen later, it is necessary to use three sublattices—a, b, and c—to distinguish the possible ordered states. With these definitions the van der Waals term h_{vdW} becomes

$$h_{\mathrm{vdW}} = -\epsilon_{\mathrm{vdW}}(S_a^2 S_b^2 + S_b^2 S_c^2 + S_c^2 S_a^2). \tag{3}$$

In order to obtain h_{hb} it is useful to define the spin projectors

$$P_{\pm}(S_k) = \frac{1}{2}(S_k^2 \pm S_k), \tag{4}$$

which give 1, if the spin S_k is equal to the projector's subscript, or 0, if different. Using the labels of sublattices and the spin values of particle orientations as in Fig. 1, h_{hb} and h_{μ} of Eq. (2) become

$$h_{\mathrm{hb}} = -\epsilon_{\mathrm{hb}}[P_-(S_a)P_+(S_b) + P_-(S_b)P_+(S_c) + P_-(S_c)P_+(S_a)] \tag{5}$$

and

$$h_{\mu} = -\frac{\mu}{3}(S_a^2 + S_b^2 + S_c^2). \tag{6}$$

Note that every site is shared by six triangles, and the factor of 1/3 has been used here to absorb the contribution of the chemical potential in a single triangle in Eq. (2). Using Eqs. (3)–(6), and grouping the terms by the order of spin coupling, we get

$$h_{\mathrm{BL}} = \frac{\epsilon_{\mathrm{hb}}}{4}(S_aS_b + S_bS_c + S_cS_a) - \left(\epsilon_{\mathrm{vdW}} + \frac{\epsilon_{\mathrm{hb}}}{4}\right) \times (S_a^2S_b^2 + S_b^2S_c^2 + S_c^2S_a^2) - \frac{\mu}{3}(S_a^2 + S_b^2 + S_c^2) - \frac{\epsilon_{\mathrm{hb}}}{4}(S_a - S_b)(S_b - S_c)(S_c - S_a). \tag{7}$$

As noted previously by Young and Lavis [35], the Hamiltonian of Eq. (7) is obtained by adding an anisotropic interaction given by

$$h_{\mathrm{ani}} = \frac{\epsilon_{\mathrm{hb}}}{4}(S_a - S_b)(S_b - S_c)(S_c - S_a). \tag{8}$$

to the BEG Hamiltonian

$$h_{\mathrm{BEG}} = -J(S_aS_b + S_bS_c + S_cS_a) - K(S_a^2S_b^2 + S_b^2S_c^2 + S_c^2S_a^2) + \frac{\Delta}{3}(S_a^2 + S_b^2 + S_c^2). \tag{9}$$

The parameters of the BEG Hamiltonian are related to the fluid parameters of the BL model through

$$J = -\frac{\epsilon_{\mathrm{hb}}}{4} < 0, \tag{10a}$$

$$K = \epsilon_{\mathrm{vdW}} + \frac{\epsilon_{\mathrm{hb}}}{4}, \tag{10b}$$

$$\Delta = -\mu. \tag{10c}$$

From Eq. (10a)–(10c) it follows that hydrogen bonds in the BL model are in some way connected to antiferromagnetism, since $J=-\epsilon_{\mathrm{hb}}<0$. This relation will be discussed further in Sec. V.

To allow the comparison with the equivalent isotropic model we define an interpolating Hamiltonian

$$h_I(\lambda) = h_{\mathrm{BEG}} + \lambda h_{\mathrm{ani}}, \tag{11}$$

which reproduces the BEG or the BL Hamiltonian on the triangular lattice, by setting λ equal to 0 or 1, respectively [54].

In addition, it will be convenient to define two interpolating parameters: the reduced interaction strength

$$\zeta(\lambda) = \frac{K - \lambda|J|}{(1+3\lambda)|J|} \tag{12}$$

and the reduced chemical potential

$$\mu^*(\lambda) = -\frac{\Delta}{(1+3\lambda)|J|} \tag{13}$$

with J and K defined as in Eqs. (9). Thus, for the BL model we have $\zeta(1)=\epsilon_{\mathrm{vdW}}/\epsilon_{\mathrm{hb}}$ and $\mu^*(1)=\mu/\epsilon_{\mathrm{hb}}$, while for the BEG model Eqs. (12) and (13) yield $\zeta(0)=K/|J|$ and $\mu^*(0)=-\Delta/|J|$. Since these parameters have been *chosen* to univocally describe the corresponding ground states of the two models, the λ dependence of $\zeta(\lambda)$ and $\mu^*(\lambda)$ will be left implicit. From now on, reference to ζ and μ^* implies use of Eqs. (12) and (13), with $\lambda=1$ for analysis of the BL model, and $\lambda=0$ for analysis of the BEG model.

A first insight into the similarities of the models can be obtained by inspecting possible spin states on a single triangle. Assuming that null temperature microstates are composed of the ordered repetition of triangle configurations (with the allowed degeneracies), one may calculate the corresponding ground state grand potentials. This assumption leads to four possible stable fluid phases for the BL model, at null temperature [gas (G), high-density liquid (HDL), low-density liquid (LDL), and intercalated (I)], which may be mapped onto magnetic phases displayed by the BEG model [paramagnetic (P), frustrated paramagnetic (FP), antiferromagnetic (AF), and antiquadrupolar (AQ)]. Possible configurations for the different phases we propose are illustrated in Fig. 2. The high-density liquid phase is in fact highly degenerate. The free-energies per particle of the two HDL configurations represented in the figure are easily shown to be equal. These two and every configuration derived from the LDL structure by filling up some fraction θ of the empty sites coexist at $\zeta=-\mu^*/6$. From now on we will take advantage of the relation between the two models, and all the references to thermodynamic phases of the BEG model will use the fluid notation.

The spectra of the interpolating Hamiltonian H_I are shown in Table I, with fluid nomenclature indicated in the first column. Ground state phase transition lines can be obtained from comparison of the grand potentials of Table I and it can be noted that the $T=0$ phase diagrams of the two models present the same topology, as shown in Fig. 2. The HDL and gas phases exist at some region of μ^*, for all values of ζ. There is a triple point at $(\mu^*=2,\zeta=1/3)$ indicating the appearance of a low-density liquid phase. This phase will be stable at some interval of μ^* for $\zeta<1/3$ and will coexist with the gas phase for interaction strengths in the range $-1<\zeta<1/3$, until the appearance of another triple point at $(\mu^*=0,\zeta=-1)$. This triple point is related to the stability of the intercalated phase, and occurs only when the van der Waals interaction is repulsive and stronger than the hydrogen bond interaction in the BL model, i.e., when the overall interaction between molecules is repulsive.

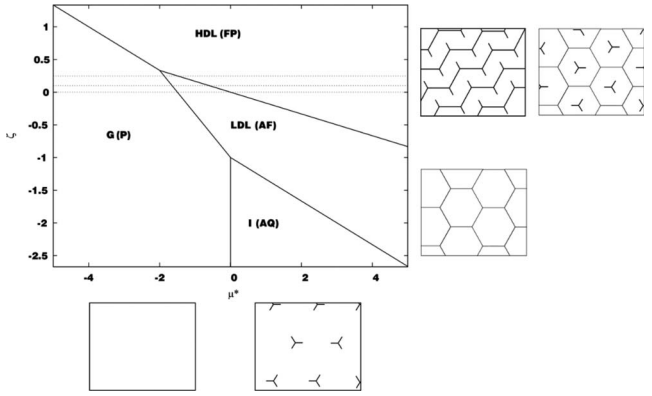

FIG. 2. Ground state of the Bell-Lavis and the antiferromagnetic Blume-Emery-Griffiths models (with a single triangle taken as a unitary cell) in terms of reduced interaction strengh ζ and reduced chemical potential μ^*. Representative configurations of the Bell-Lavis model are shown on the sides of the diagram, with straight lines representing hydrogen bonds. The degenerate HDL (FP) phase is represented by two of the many possible configurations (see text for phase names). Dotted lines indicate the parameters ($\zeta=1/4$, 1/10, and 0) studied in this work.

Despite the topological equivalence between the ground states of the BL and BEG models, there is an important difference between the LDL phase and the antiferromagnetic phase which is caused by the anisotropic interaction term in Eq. (8). As can be seen in Table I, the only states that have been changed by this term were the low-density liquid and the unbonded low-density liquid (both antiferromagnetic states), whose "microscopic" grand potentials per triangle differ by $\Delta H=-4\lambda J=\lambda\epsilon_{\mathrm{hb}}$. By making $\lambda=0$ these states merge into the antiferromagnetic state, indicating that the major effect of the anisotropy is to distinguish between low-density bonding and nonbonding states, thus breaking the degeneracy of the antiferromagnetic states. This is illustrated in Fig. 1, in which all states represented are antiferromagnetic, whereas for the liquid, only (a) represents bonded states, of lower energy, while (b) represents nonbonding states, of higher energy.

III. EXACT SOLUTION ON THE BETHE LATTICE

The BL and BEG models are studied here using a recursive approach [52] to the Bethe lattice [50]. The Bethe lattice

TABLE I. Ground state of the effective Hamiltonian in Eq. (11), under the hypothesis discussed in the text. Stable and unstable configurations are shown with fluid names, microscopic grand potentials (using fluid and magnetic parameters in different columns), degeneracy Ω, density ρ, the number of hydrogen bonds per particle ρ_{hb}, the equivalent quantity for the BEG model $\Delta\rho_f$, and illustrative spin representations. The *unbonded LDL* is emphasized because it is unstable in the BL model but is stable, and equal to the LDL, in the antiferromagnetic BEG model.

	$H_I(S_a,S_b,S_c)$						
Fluid phase	Fluid	Magnetic	Ω	ρ	ρ_{hb}	$\Delta\rho_f$	(S_a,S_b,S_c)
Stable phases							
Gas	0	0	1	0	0	0	(0,0,0)
HDL	$-\epsilon_{\mathrm{hb}}-3\epsilon_{\mathrm{vdW}}-\mu$	$J-3K+\Delta$	6	1	1	1	$(+,-,\pm)$
LDL	$-\frac{(1+\lambda)}{2}\epsilon_{\mathrm{hb}}-\epsilon_{\mathrm{vdW}}-\frac{2}{3}\mu$	$(1+2\lambda)J-K+\frac{2}{3}\Delta$	3	2/3	3/2	3/2	$(+,-,0)$
Intercalated	$-\frac{1}{3}\mu$	$\frac{1}{3}\Delta$	6	1/3	0	0	$(0,\pm,0)$
Unbonded LDL	$-\frac{(1-\lambda)}{2}\epsilon_{\mathrm{hb}}-\epsilon_{\mathrm{vdW}}-\frac{2}{3}\mu$	$(1-2\lambda)J-K+\frac{2}{3}\Delta$	3	2/3	0	3/2	$(-,+,0)$
Unstable phases							
Densely ordered	$-3\epsilon_{\mathrm{vdW}}-\mu$	$-3J-3K+\Delta$	2	2/3	0	$-3/2$	$(+,+,+)$
Lightly ordered	$-\epsilon_{\mathrm{vdW}}-\frac{2}{3}\mu$	$-J-K+\frac{2}{3}\Delta$	6	1	0	-1	$(+,0,+)$

is known to capture the essential features of different models, particularly when the usual mean field treatment fails [50]. On the recursive approach, the system is studied in an infinite hierarchical tree, which here is the sequential Husimi cactus, and the thermodynamical properties are calculated on the interior of this tree by iterating a set of recursion relations until a fixed point is reached.

A triangular lattice may be represented by a Husimi cactus of coordination $q=6$. This is achieved by letting the branches of the cactus grow indefinitely, and attaching the base sites of two branches to each vertex of the central triangle. Figure 3 shows two branches of the Husimi cactus that were grown for three generations: one constructed with the usual symmetrical procedure and the other through a sequential procedure [51]. While in the symmetrical procedure all generations grow simultaneously from the central triangle, in the sequential procedure generations starting on different sublattices are grown in a sequence which specifies the order in which sublattices are added in the growth process. Here we adopt this order as $a\rightarrow b\rightarrow c\rightarrow a$.

In the next section we present a set of recursion relations that describe a general spin-1 Hamiltonian on the sequential Husimi cactus and give an expression for the grand potential of this system in the interior of the cactus.

A. Recursive approach to a general spin-1 Hamiltonian on the sequential Husimi cactus

Let us consider the general Hamiltonian $h(S_a,S_b,S_c)$ on a single triangle. The partition function of a sequential Husimi cactus with M generations, and growth starting in generation 0 on sublattice a of a central triangle, is given by

$$\Xi_{0,1,2}^{(M)}=\sum_{S_a,S_b,S_c} e^{-\beta h(S_a,S_b,S_c)}\Lambda_0^2(a,S_a)\Lambda_1^2(b,S_b)\Lambda_2^2(c,S_c), \tag{14}$$

where $\beta=1/k_BT$. $\Lambda_k(l,S_l)$ is the partition function of a branch of the cactus starting at a site of sublattice l on generation k, in state spin s_l, whose child branches will grow sequentially for $m-k$ generations. Due to the cactus's self-similarity, the partition functions of branches on sucessive generations satisfy the following equations:

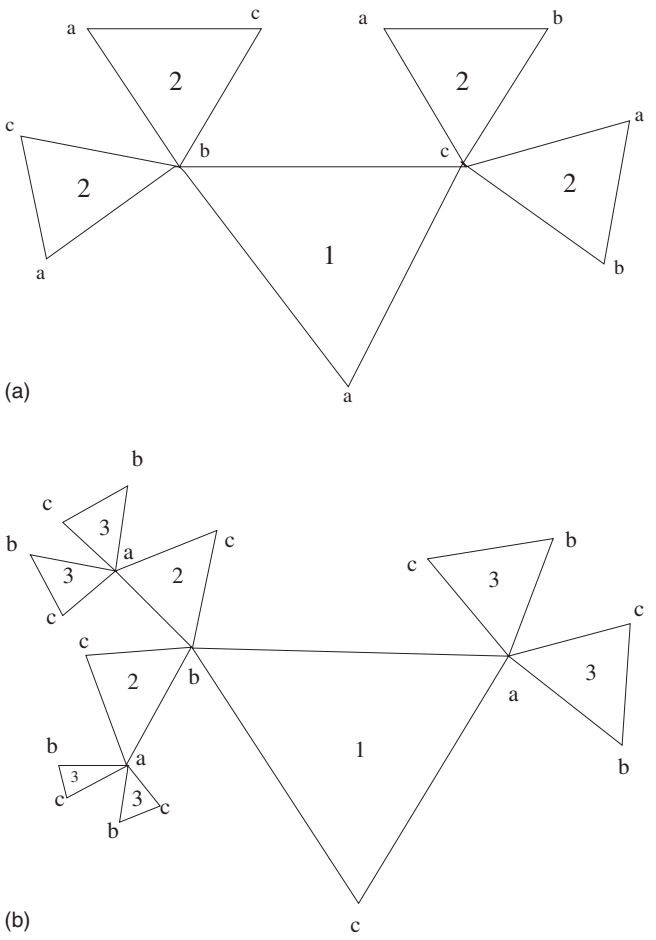

FIG. 3. (a) Symmetrical and (b) sequential constructions of the branches of the Husimi cactus.

$$\Lambda_k(a,S_a) = \sum_{S'_b,S'_c} e^{-\beta h(S_a,S'_b,S'_c)} \Lambda^2_{k+1}(b,S'_b)\Lambda^2_{k+2}(c,S'_c), \tag{15a}$$

$$\Lambda_k(b,S_b) = \sum_{S'_c,S'_a} e^{-\beta h(S'_a,S_b,S'_c)} \Lambda^2_{k+1}(c,S'_c)\Lambda^2_{k+2}(a,S'_a), \tag{15b}$$

$$\Lambda_k(c,S_c) = \sum_{S'_a,S'_b} e^{-\beta h(S'_a,S'_b,S_c)} \Lambda^2_{k+1}(a,S'_a)\Lambda^2_{k+2}(b,S'_b). \tag{15c}$$

Normalization of the probabilities on each sublattice reduces the initial nine equations, resulting from the three possible states for S_l, to six equations. The definition

$$\Lambda_k(l,S_l) = B_k(l) x_k(l,S_l)^{S_l^2} \tag{16}$$

may be used to rewrite Eqs. (15a)–(15c) as a dynamical mapping on the partial partition functions $x_k(l,S_l)$, given by

$$x_k(a,S_a) = \frac{f_{(k+1,k+2)}(a,S_a)}{f_{(k+1,k+2)}(a,0)}, \tag{17a}$$

$$x_k(b,S_b) = \frac{f_{(k+1,k+2)}(b,S_b)}{f_{(k+1,k+2)}(b,0)}, \tag{17b}$$

$$x_k(c,S_c) = \frac{f_{(k+1,k+2)}(c,S_c)}{f_{(k+1,k+2)}(c,0)}. \tag{17c}$$

The functions $f_{(m,n)}(l,S_l)$ are

$$f_{(m,n)}(a,S_a) = \sum_{S'_b,S'_c} e^{-\beta h(S_a,S'_b,S'_c)} x_m^{2S'^2_b}(b,S'_b) x_n^{2S'^2_c}(c,S'_c), \tag{18a}$$

$$f_{(m,n)}(b,S_b) = \sum_{S'_c,S'_a} e^{-\beta h(S'_a,S_b,S'_c)} x_m^{2S'^2_c}(c,S'_c) x_n^{2S'^2_a}(a,S'_a), \tag{18b}$$

$$f_{(m,n)}(c,S_c) = \sum_{S'_a,S'_b} e^{-\beta h(S'_a,S'_b,S_c)} x_m^{2S'^2_c}(a,S'_a) x_n^{2S'^2_b}(b,S'_b). \tag{18c}$$

Note that $x_k(l,0)$ and $B_k(l)$ do not appear in Eqs. (18) due to definition (16). The functions $B_k(l)=\Lambda_k(l,0)$ satisfy some recursion relations which will be used later to obtain the grand potential. For $l=a$ this relation is

$$B_k(a) = B^2_{k+1}(b)B^2_{k+2}(c) f_{(k+1,k+2)}(a,0). \tag{19}$$

The set of Eqs. (16) are iterated sequentially, starting from large M values, until a fixed point is found. The existence of more than one fixed point, which can be obtained using different initial values in Eqs. (16), indicates the presence of various phases. The region of stability of each phase is established by comparing grand potentials. In the neighborhood of any fixed point we will have, for $k \ll M$, $x_k(l,S_l) = x_{k-1}(l,S_l) = x(l,S_l)$. From now on the subscript k will be avoided on the partial partition functions $x(l,S_l)$ and it will be assumed that their values are obtained on the interior of the cactus tree.

An analytical expression for the grand potential may be obtained by following Gujrati's proposal [50], in which it is assumed that the grand potential of the cactus is additive in the contributions from surface and bulk sites. Moreover, it is also assumed [50] that the surface grand potential of a cactus with M generations is equal to the grand potential of a certain number r of cactus with $M-1$ generations, with r being the ratio of the numbers of surface sites on trees with successive M. For the $q=r+1=6$ symmetrical Husimi cactus, the bulk grand potential per unit area, ϕ, is given by

$$\phi = \frac{\Phi}{A} = \frac{\Phi_0^{(M)} - r\Phi_0^{(M-1)}}{\delta a_0}, \tag{20}$$

where $\delta=3$ is the difference, in site number, between one cactus with M generations and the $r=4$ cactus with $M-1$ generations, and $A=\delta a_0$ with a_0 being the area of a single site. For the sequential Husimi cactus this quantity will be slightly different because each branch starts in different generation. Using the growth definition adopted here, ϕ for the sequential Husimi cactus is written as

$$\phi = \frac{\Phi}{A} = \frac{\Phi^{(M)}_{0,1,2} - 2\Phi^{(M-1)}_{3,1,2} - 2\Phi^{(M-2)}_{3,4,2}}{3a_0}. \tag{21}$$

To obtain an expression for ϕ in terms of the partial partition functions $x_k(a,S_a)$, it is convenient to write

$$\Xi^{(M)}_{0,1,2} = B_0^2(a)B_1^2(b)B_2^2(c)\sum_{S_a} x^{2S_a^2}(a,S_a) f(a,S_a), \tag{22}$$

where the subscript k may be omitted in $f(a,S_a)$ because $k \ll M$.

The grand potential per unit of area is obtained using the relation $\Xi = e^{-\beta\Phi}$ and applying Eqs. (19) and (22) on Eq. (21). After some algebra, this procedure leads to

$$\phi = -\frac{k_B T}{3a_0} \ln\left(\prod_{l=a,b,c} \frac{f(l,0)}{\sum_{S_l} x(l,S_l)^{3S_l^2}} \right). \tag{23}$$

Finally, the pressure at given temperature T and chemical potential μ is simply $P=-\phi$. In what follows we introduce the mean value of some quantities necessary for the analysis of Sec. IV.

B. Mean values In the interior of the cactus

To obtain the mean value of some properties it will be useful to write the probability of finding a molecular configuration with given spin values S_a, S_b, and S_c in the interior of the cactus:

$$P(S_a,S_b,S_c) = \frac{e^{-\beta H_I(S_a,S_b,S_c)} x^{2S_a^2}(a,S_a) x^{2S_b^2}(b,S_b) x^{2S_c^2}(c,S_c)}{\sum_{S_a',S_b',S_c'} e^{-\beta H_I(S_a',S_b',S_c')} x^{2S_a'^2}(a,S_a') x^{2S_b'^2}(b,S_b') x^{2S_c'^2}(c,S_c')}. \quad (24)$$

This definition implies that the mean value of any function $g(S_a,S_b,S_c)$ will be simply

$$\langle g(S_a,S_b,S_c)\rangle = \sum_{S_a,S_b,S_c} g(S_a,S_b,S_c) P(S_a,S_b,S_c). \quad (25)$$

Thus, the density on the central triangle is given by

$$\rho = \frac{1}{3} \sum_{l=a,b,c} \langle S_l^2 \rangle, \quad (26)$$

and the mean energy per particle of the interpolating Hamiltonian [Eq. (11)] is

$$u(\lambda) = \frac{1}{\rho} \langle h_I(\lambda) - h_\mu \rangle, \quad (27)$$

with $h_I(\lambda)$ and h_μ from Eqs. (11) and (6), respectively.

A quantity that is relevant for the particular case of the BL model is the number of hydrogen bonds per particle:

$$\rho_{\mathrm{hb}} = -\frac{1}{\epsilon_{\mathrm{hb}}\rho} \langle H_{\mathrm{hb}} \rangle. \quad (28)$$

At this point it is interesting to define a quantity similar to ρ_{hb}, in the context of the BEG model. Before doing this, let us note that the mean number of nearest neighbors per particle is

$$\rho_{\mathrm{NN}} = \frac{1}{\rho} \langle S_a^2 S_b^2 + S_b^2 S_c^2 + S_c^2 S_a^2 \rangle, \quad (29)$$

and that using this definition Eq. (27) becomes

$$u(\lambda = 1) = u_{\mathrm{BL}} = -\epsilon_{\mathrm{hb}} \rho_{\mathrm{hb}} - \epsilon_{\mathrm{vdW}} \rho_{\mathrm{NN}} \quad (30)$$

for the BL model, with $\lambda = 1$, and

$$u(\lambda = 0) = u_{\mathrm{BEG}} = -|J| \left(-\frac{1}{\rho} \langle S_a S_b + S_b S_c + S_c S_a \rangle \right) - K \rho_{\mathrm{NN}} \quad (31)$$

for the antiferromagnetic BEG model, with $\lambda = 0$.

By comparing Eqs. (30) and (31) one realizes that the quantity

$$\Delta\rho_f = -\frac{1}{\rho} \langle S_a S_b + S_b S_c + S_c S_a \rangle \quad (32)$$

has an energetic meaning in the BEG model that is equivalent to the density of hydrogen bonds in the BL model. It is worth mentioning that $\Delta\rho_f$ presents the desired behavior at $T=0$, i.e., $\rho_{\mathrm{hb}} = \Delta\rho_f$ for all stable states of Table I, and that the unbonded low-density liquid becomes equal to the LDL phase in the BEG model. Nevertheless, the definitions ρ_{hb} and $\Delta\rho_f$ are not equal for unstable configurations at $T=0$, e.g., for the densely oriented and lightly oriented states in Table I $\rho_{\mathrm{hb}}=0$ but $\Delta\rho_f=-1$ in the latter and $\Delta\rho_f=-3/2$ in the former.

Another relevant extensive property is the entropy per particle, which can be calculated numerically from the expression of the grand potential in Eq. (21) and is written as

$$s = -\frac{1}{N}\frac{\partial \Phi}{\partial T} = -\frac{1}{\rho}\frac{\partial \phi}{\partial T}, \quad (33)$$

where N is the number of particles in a system with fixed area A.

IV. PHASE DIAGRAMS AND THERMODYNAMIC PROPERTIES

To begin our analysis we compare the finite-temperature pressure-temperature phase diagrams of the two models for three values of reduced interaction strength $\zeta = 1/4$, 1/10, and 0, as shown in Fig. 4. These values were chosen in the interval $0 \le \zeta < 1/3$, which satisfies the stability condition for the LDL phase and the restriction of an attractive van der Waals interaction (or biquadratic spin coupling, in the BEG model). The reduced units defined in Table II are used. Phase transitions, temperatures of maximum and minimum density, and the locus of null entropy are shown with different lines and symbols in this figure.

In spite of the perfect mapping of the $t=0$ phase diagram topologies, temperature introduces some distinctions between the thermodynamic behavior of the two models. The first difference we note is that the anisotropic interaction in the BL model favors the LDL, since this phase is stable at larger temperatures and pressures, in comparison to the antiferromagnetic phase of the BEG model. This may be related to the behavior of the entropy. The latter can be inferred by applying the Clausius-Clapeyron equation to the liquid-liquid coexistence line. At higher temperatures, both models present a more entropic HDL phase, as compared to the LDL phase. At lower temperatures, however, the BL model presents a more entropic LDL, as compared to HDL, which may explain the improvement of the stability of the LDL. This result is somewhat unexpected because in the ground state analysis of Sec. II it was found that the number of states of the LDL phase, in the BL model, was half the degeneracy of the BEG model.

Both models exhibit a coexistence line between the gas and HDL phases, ending in a critical point. The position of this point, (t_c, p_c), goes to lower temperature and pressure as the intensity of the van der Waals interaction (biquadratic spin coupling) is lowered. In the BL model this shift produces noticeable changes in the phase diagram, since the critical point concerned crosses the gas-LDL transition, becoming metastable at some ζ' in the interval $1/4 < \zeta' < 1/10$.

A density anomaly was searched for in the HDL phase. Lines of maximum density are shown in Fig. 4 and display similar behavior for equal ζ, in both models. The TMD line meets the LDL-HDL coexistence, at null temperature and at pressure $p=1$. An important point to note is that, in the BL model, the lines of maximum densities are always in the metastable HDL phase. As to the BEG model, the TMD oc

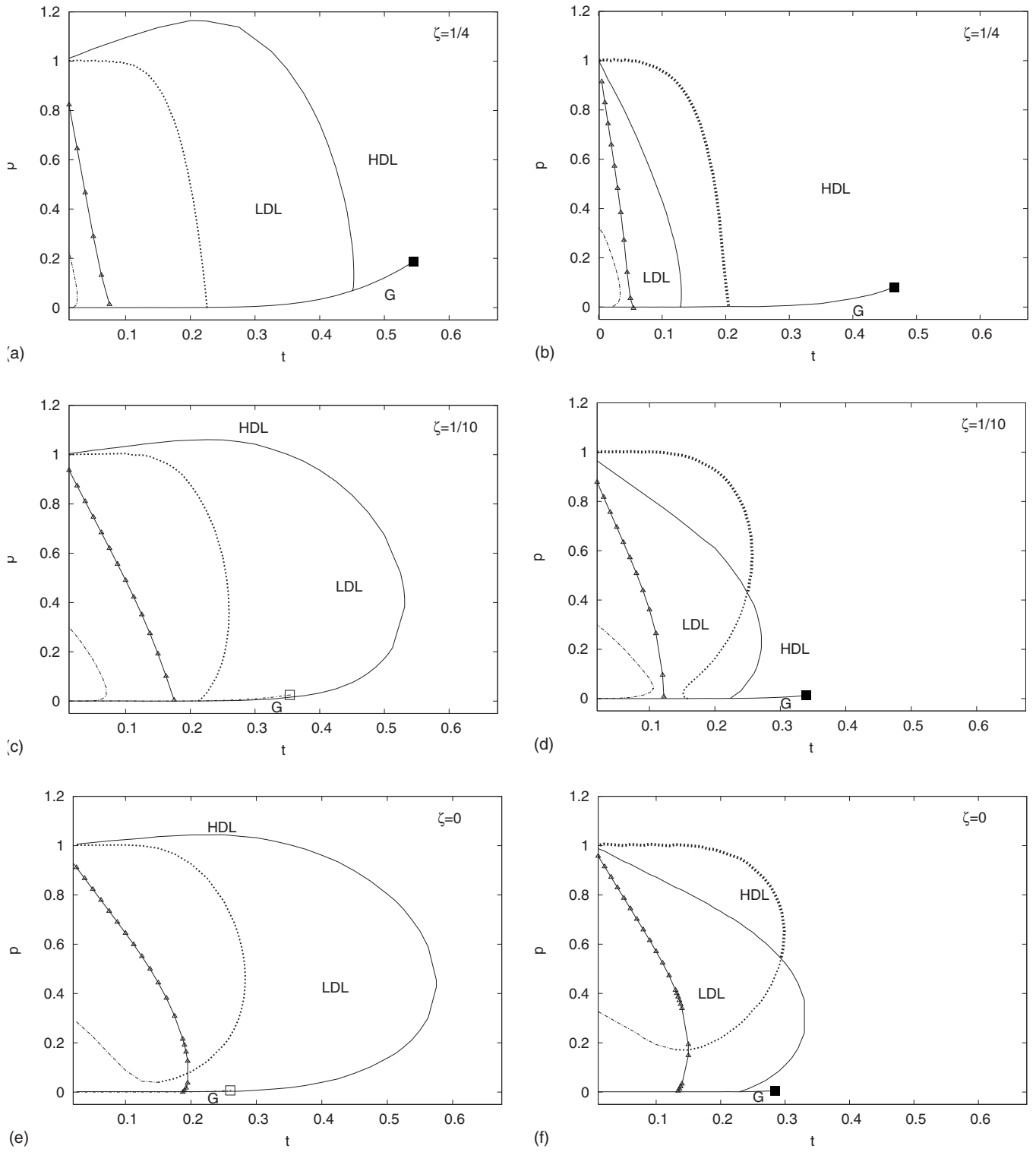

FIG. 4. Reduced temperature vs pressure phase diagrams of the Bell-Lavis (left) and antiferromagnetic Blume-Emery-Griffiths (right) models compared with reduced interaction strength ζ values 1/4, 1/10, and 0. Phases are indicated in fluid notation as G (gas), HDL (high-density liquid), and LDL (low-density liquid). Phase coexistences are represented by a line and the critical point of the coexistence between gas and HDL is marked with a square. Note that an unfilled square has been used to indicate the metastability of this point in (c) and (e). The loci of stable maximum, metastable maximum, and metastable minimum density in the HDL phase are shown with thick dotted, thin dotted, and dash-dotted lines, respectively. A line connected with triangles indicates the temperatures, on each graphic, below which the entropy in the HDL phase is negative.

TABLE II. Definition of the reduced variables used for the Bell-Lavis and antiferromagnetic Blume-Emery-Griffiths models.

	BL	BEG
t	k_BT/ϵ_{hb}	$k_BT/\lvert J\rvert$
p	$Pa_0/(\epsilon_{hb}-3\epsilon_{vdW})$	$Pa_0/(\lvert J\rvert-3K)$
k_t	$(\epsilon_{hb}-3\epsilon_{vdW})k_T/a_0$	$(\lvert J\rvert-3K)k_T/a_0$
c_v	c_V/k_B	c_V/k_B
c_p	c_P/k_B	c_P/k_B

curs in a stable HDL phase, for $\zeta=1/4$, and partly in stable and partly in metastable regions of the HDL phase, for $\zeta=1/10$ and 0.

Lines of minimum density were also found for both models, at lower temperatures, in the metastable HDL phase (see Fig. 4).

For $\zeta=1/4$, the BL metastable TMD line has a negative inclination when it meets the gas phase, at low pressures. This result is in accordance with a previous study by Bell and Lavis (Ref. [33]), in which a few curves of density, as functions of temperature, at fixed pressure, are shown.

For $\zeta=1/10$, the line of minimum density is shifted to higher temperatures and the TMD line returns to lower temperatures, at low pressures. In the case of the BEG model, the derivative of the TMD line changes its sign twice, retracing toward higher temperatures, just before meeting the gas phase.

For $\zeta=0$, the lines of maximum and minimum density merge into a single curve, at a minimum of that line. A similar behavior has been observed with differerent orientational models (see Fig. 4 of Ref. [37] and Fig. 5 of Ref. [44]). In both BEG and BL models, a single locus of extremum densities appears at some value of ζ between 1/10 and 0, probably at a higher value of ζ for the BEG model, due to the proximity of the two lines shown in Fig. 4(d). Under the $\zeta=0$ condition the BEG model corresponds to the antiferromagnetic Blume-Capel model.

Analogously to other cases, the analytical solutions from Bethe-like approaches [55] may present a region in the phase diagram with unphysical solutions of negative entropy. We observe such a region in the metastable HDL, for all the investigated values of ζ, as shown in Fig. 4. By inspecting these regions of negative entropy, it can be concluded that the observed minimum in density is unphysical in both models, at least within the approximation used in this work.

A. The $\zeta=1/4$ case

From now on let us consider the case $\zeta=1/4$ in detail. Figure 5 displays the density vs temperature phase diagrams. Only phase coexistence lines, both stable and metastable, TMD lines, and the triple point have been shown, for clarity.

In the BL model, the density anomaly occurs in a metastable regime and a reentrance can be noted in the metastable continuation of the gas-HDL coexistence, when the TMD line encounters it. The null temperature limit of the metastable TMD line is at density $\rho_0'=0.976\pm0.016$, which is

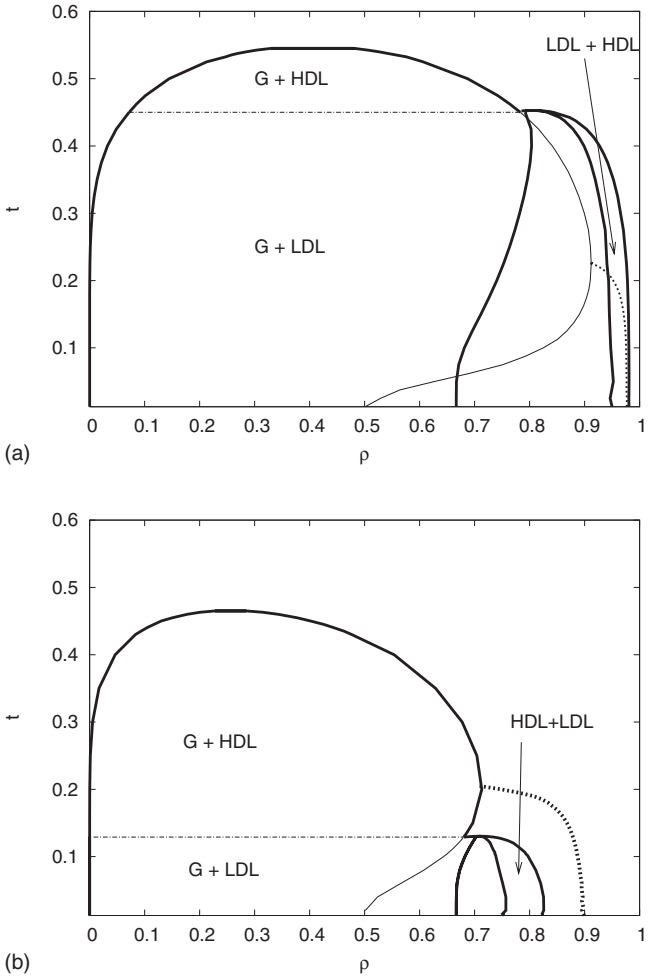

FIG. 5. Reduced temperature vs density phase diagram of the (a) Bell-Lavis and (b) antiferromagnetic Blume-Emery-Griffiths models with the reduced interaction strength value $\zeta=1/4$. Labels are the same used in Fig. 4. Phase transitions and the metastable continuation of the coexistence between gas and HDL are shown with thick and thin lines, respectively. The temperature of maximum densities and the triple point are shown with dotted and dash-dotted line, respectively.

compatible with the value $\rho_0=0.9763$, found by Lavis for the $t=0$ and $p=1$ limits [33]. The coexistence between LDL and HDL is very thin and occurs mostly at densities larger than 0.7. Near to the triple point there is an azeotropic point, at which two regions of coexistence meet. This point is related to the existence of a region with reversed relative densities, in the liquid phases, and corresponds to a very small region in which the derivative of the coexistence line dp_{coex}/dt, is positive.

In the BEG model the TMD line meets the gas-HDL phase coexistence in a stable regime and a reentrance can be noted in this coexistence too, as shown in Fig. 5(b). The null temperature limit of the TMD line happens at a density $\rho_0''=0.89\pm0.025$. The LDL-HDL coexistence lies at lower temperatures and lower densities, when compared to the equivalent liquid-liquid coexistence, in the BL model. Again, near to the triple point there is an azeotropic point that can be visualized in Fig. 6. In the BEG model, the region of re-

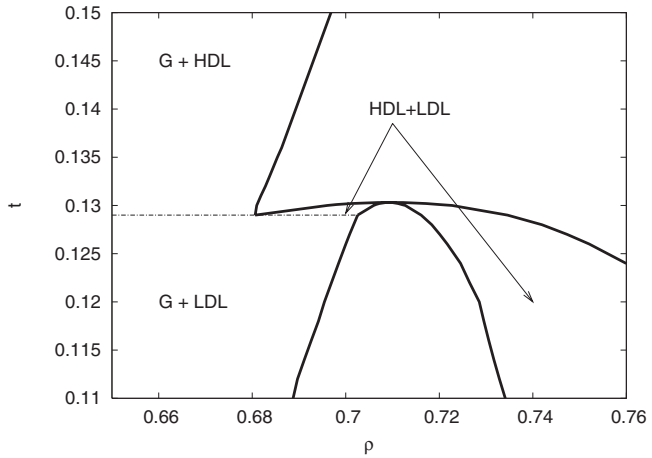

FIG. 6. Reduced temperature vs density phase diagram of the antiferromagnetic Blume-Emery-Griffiths model shown in Fig. 5 in the neighborhood of the triple point. Labels are the same used in Figs. 4 and 5.

versed densities in the LDL-HDL coexistence is larger, corresponding to $dp_{\mathrm{coex}}/dt>0$ in a wider pressure interval.

At the $t=0$ limit, the LDL density at gas-LDL coexistence goes to 2/3, for both models, whereas the metastable continuation of the gas-HDL coexistence line yields density 1/2. The density 2/3 was used in the ground state analysis of Sec. II, in order to predict the existence of the LDL phase. This analysis provided the values $p=0$ and 1 for the gas-LDL and the LDL-HDL transitions, respectively, which are the same values found in the phase diagrams of Fig. 4. However, from the Husimi cactus calculations, the $t=0$ limit for the LDL density at the LDL-HDL coexistence line is $\rho_{\mathrm{LDL}}=0.95\pm0.005$. On the HDL side we have found $\rho_{\mathrm{HDL}}=0.98\pm0.0005$. These densities are somewhat different from the values $\rho'_{\mathrm{LDL}}=0.8963$ and $\rho'_{\mathrm{HDL}}=0.9763$, found at $t=0$ in the approximation used by Lavis [34]. For the BEG model, the corresponding densities are $\rho''_{\mathrm{LDL}}=0.75\pm0.03$ and $\rho''_{\mathrm{HDL}}=0.83\pm0.02$.

In Fig. 7 structural properties in the HDL phase of the models are compared at equivalent pressures as functions of temperature. At null temperature, the quantities of both models converge to the same values, except for the entropy at small pressures. A density anomaly is present for all pressures $p<1$, but the temperature of maximum density reaches denser states in the BL model. Concomitant with the density increase, there is a steep decrease in the density of hydrogen bonds ρ_{hb} and the corresponding quantity in the BEG model, $\Delta\rho_f$. This decrease is less steep in the BEG case, accompanying a smaller density increase. The entropy per particle is higher for the BEG model, generally, but at higher pressures ($p>1$) and at the null temperature limit, it converges to a finite value that is identical in both BL and BEG models. This residual entropy is associated with the degeneracy of the ground state, which allows for several configurations to present the same free energy in this region.

The behavior of thermodynamic response functions in the HDL phase are compared for both models in Fig. 8. Isothermal compressibilities, shown in Figs. 8(a) and 8(b), present maxima at pressures $p<1$, which increase in magnitude as pressure $p=1$ is approached. The isobaric heat capacities also present peaks whose positions are dislocated to lower temperatures, accordingly. The isovolumetric heat capacities display maxima at low pressures, with peak size decreasing as pressure is increased, and eventually disappearing on approaching $p=1$.

V. DISCUSSION

We have shown that a line of maximum densities exist in a wide region of pressures and temperatures for both the BL and the BEG models (see Fig. 4), with reduced interaction strengths in the range

$$0\leq\zeta\leq1/4. \tag{34}$$

We emphasize the meaning of the above inequality. The $0\leq\zeta$ condition reflects the requirement of a physically relevant attractive van der Waals interaction. At the other end, the condition $\zeta\leq1/4$ guarantees the stability of the LDL phase at $t=0$ ($\zeta<1/3$; see Fig. 2).

The existence of the LDL phase seems to be a *necessary* condition for the presence of a density anomaly in the BL and BEG models, because it indirectly creates a free energy competition between two liquid structures: a normal and a bonded HDL structure. The normal HDL structure occurs at higher pressures, while the bonded HDL arises as a metastable liquid, in the region of stability of the LDL and at low pressures ($p<1$). The "new" bonded HDL structure appears to "borrow" some properties of the LDL phase. This idea is further discussed in what follows.

A. Liquid-liquid coexistence

The stability of the LDL phase is easily established if one looks at the ground state Gibbs free energy. At null pressure and $t=0$, the free energy per particle is given by $g(p=0,t=0)=u$ and the gas will coexist with the liquid phase of lower energy. Inspection of Table I shows that the LDL phase has lower energy than the HDL phase if the energy of each hydrogen bond is at least three times the energy of the van der Waals interaction. For systems under this condition, as the pressure increases, there will be a point at which work performed by the compression suppresses the free energy difference between the different liquids. At this point, i.e., at $p=1$, the system passes through coexistence, and enters the HDL liquid phase.

For finite temperatures, both models present a narrow liquid-liquid phase transition as shown in the density vs temperature phase diagrams of Figs. 5 and 6. In the case of the BL model, this transition has been a matter of controversy. It was found in an early study by Lavis to be of first order, in an approximation scheme with three sublattices [33], but subsequent studies [36] based on the real space renormalization group yielded a second-order phase transition. More recently, Patrykiejew *et al.* [56] investigated, through Monte Carlo simulations, a modified version of the BL model, to which a repulsive three-body interaction was added. The main result of this work was that the transition between liquid phases occurred through a discontinuity in the specific

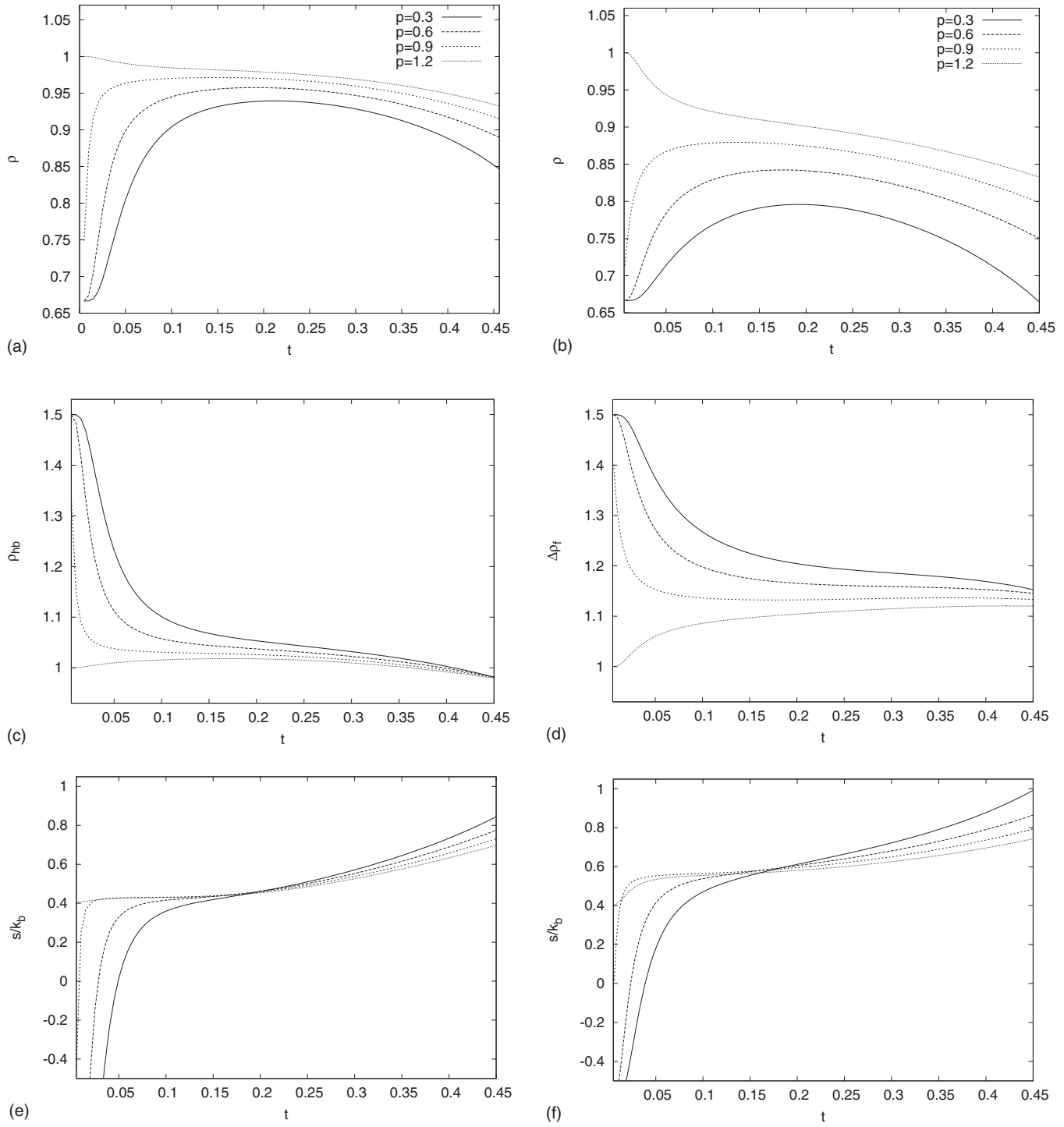

FIG. 7. Values of structural quantities, at the molecular level, of the Bell-Lavis (right) and the antiferromagnetic Blume-Emery-Griffiths models compared for the reduced interaction strength $\zeta=1/4$. From top to bottom we show (a) and (b) the density, (c) the number of hydrogen bonds per particle, (d) the quantity $\Delta\rho_f$, and (e) and (f) the entropy per particle.

heat, which would correspond to a second-order phase transition according to Ehrenfest's classification [57]. Those simulations included the original BL model, with $\epsilon_{vdW}/\epsilon_{hb}=1/4$, discussed in this study [see Fig. 4(a) in Ref. [56]].

In spite of this result, it is possible that the HDL-LDL transition of the BL model may represent another example of a weakly first-order phase transition, as in the antiferromagnetic three-state Potts model on the triangular lattice [58], or may even not exist. In order to clarify this question, additional studies are necessary, either use of a methodology that allows one to distinguish between second- and weakly first-order transitions [59], such as short-time dynamics [60], or

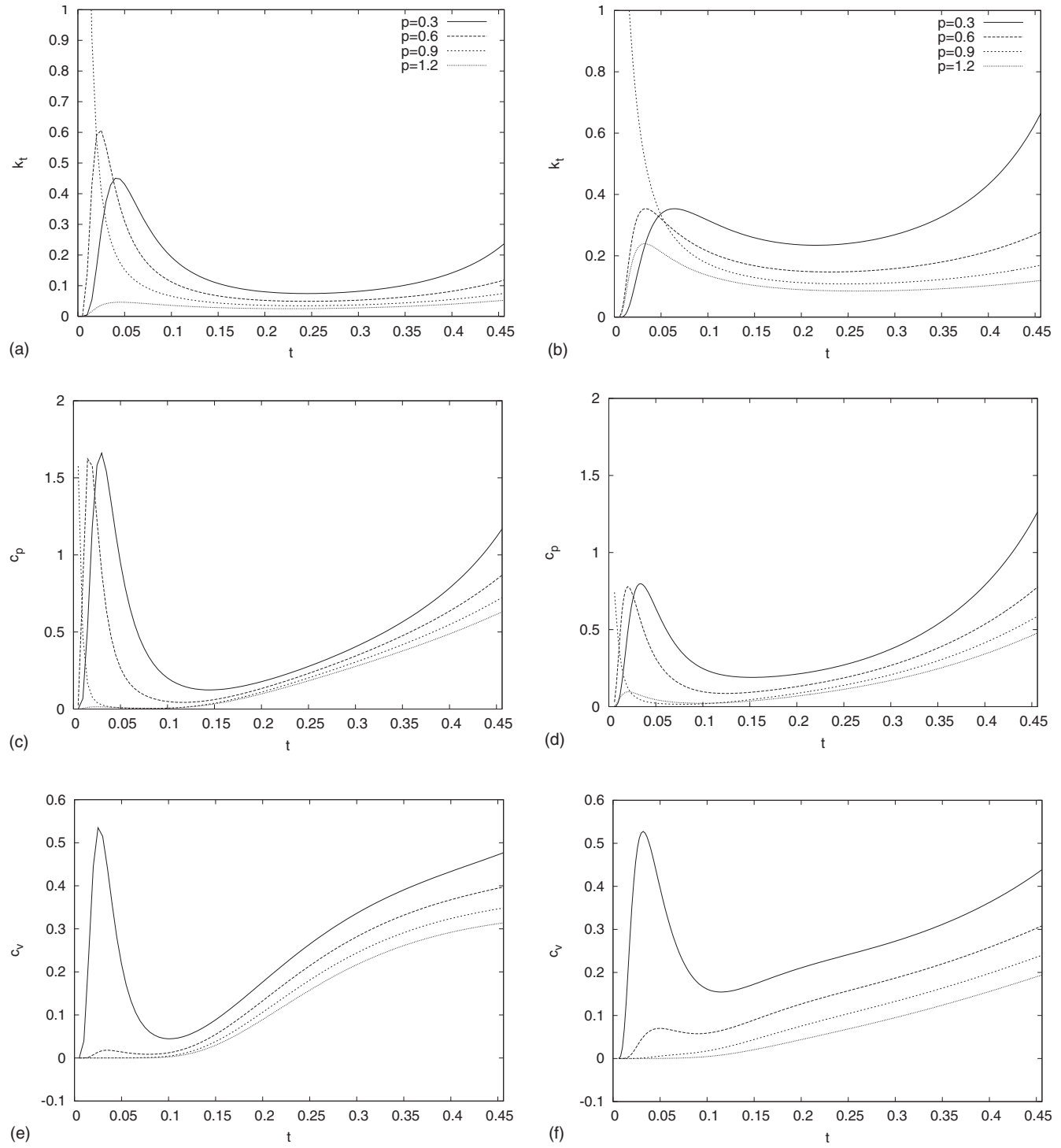

FIG. 8. Thermodynamic response functions of the Bell-Lavis (left) and the antiferromagnetic Blume-Emery-Griffiths (right) models compared for the interaction strength value $\zeta=1/4$, at constant pressure. The isothermal compressibility k_t and the constant pressure c_p and constant volume heat capacities c_v are shown from top to bottom.

investigation of the histograms of a chirality order parameter [58], which in the BL model corresponds to the anisotropic term in Eq. (8).

B. Anomalous behavior in the HDL phase

The metastability of the TMD line seems to be a major deficiency of the BL model as a model for liquid water. Nevertheless, some of the results coming from Patrykiejew's [56] Monte Carlo simulations suggest that the line of density anomalies meets the gas-HDL coexistence line in a stable region. Figure 4(a) of that work [56], the density vs temperature phase diagram for the BL model, at $\zeta=1/4$, can be compared to our results; see Fig. 5(a). In both cases, the HDL density along the gas-HDL coexistence line presents an in-

version of its slope, which represents one of the boundaries of the reentrant region.

The condition of a density increase with temperature along the coexistence curve is equivalent to an upper bound for the thermal expansion coefficient. The slope of the liquid density function $\rho(T,P)$ along the $P_{\text{coex}}(T)$ coexistence line, in the direction of increasing temperature toward the critical point can be expressed as $\partial_{\text{coex}}\rho=\sin(\theta)\rho k_T-\cos(\theta)\rho\alpha$. Where $\theta\equiv\theta(T,P)$ is the angle between the $P_{\text{coex}}(T)$ coexistence line and the T axis, k_T is the isothermal compressibility and α the isobaric expansion coefficient. Taking the liquid as denser and less entropic than the gas (i.e., $0<\theta<\pi/2$) it follows that (i) if a TMD line touches the $P_{\text{coex}}(T)$ coexistence line, the liquid density, at coexistence, must be an increasing function of temperature, at the crossing point; (ii) if the liquid density increases with temperature along the coexistence line, it is possible, but not necessary, that the coexistence line encounters the line of maximum densities; and (iii) inversely, if the liquid density decreases with temperature along the coexistence line, $\partial_{\text{coex}}\rho<0$ and $\alpha>0$, i.e., the coexistence line cannot cross any region of anomalous density behavior.

Our Bethe lattice results are in accordance with these criteria, and the meeting of the TMD line with the liquid density at coexistence (see Fig. 5) seems to coincide with the maximum liquid density, in the metastable regime (for the HDL). In Patrykiejew's Monte Carlo simulations, there are no data on the TMD, but the (stable) ρ vs T phase diagram displays a maximum for the liquid density, indicating that there might, in fact, exist a stable TMD line crossing that region.

In both the BL and the BEG models, the anomalous increase in density, at lower temperatures and for $p<1$, is accompanied by a steep decrease in the number of hydrogen bonds (or $\Delta\rho_f$, in the BEG model) as well as by a large increase in the entropy per particle, as can be seen in Fig. 7. These features are emphasized in the metastable HDL phase of the BL model. Thus the anomalous liquid in the region limited by the TMD line may be called a *bonded* HDL, to distinguish it from the *normal* HDL, which occurs at higher pressures ($p>1$) and temperatures ($t>t_{\text{TMD}}$). As stated before, the bonded HDL structure is similar to the LDL, in the sense that it is less dense and more bonded than the normal HDL structure. Nevertheless, the bonded structured liquid has the same symmetry as the HDL phase (paramagnetic) and does not have the sublattice distinction that is characteristic of the LDL (antiferromagnetic) phase. For this reason, one cannot localize the network of bonds in the bonded structure, or specify the sublattices that are filled or empty, as in the LDL.

The bonded and normal HDL structures present different mechanisms for increasing the system's entropy, as temperature rises. In the normal HDL structure, entropy is gained with an increase in the number of spatial arrangements of molecules, i.e., by increasing the molecular volume. As for the bonded HDL structure, entropy is gained, in spite of the decreasing molecular volume, due to the increase in the number of configurations for the hydrogen bond network (or in the $\Delta\rho_f$ coupling network, in the case of the BEG model) and frustration plays an important role. Frustration prevents new bonds from being created as particles are inserted to increase the density. Thus, while the number of hydrogen bonds ($\Delta\rho_f$) per particle decreases, the number of bonds per unit "volume" is almost constant (results not shown), yielding a sharp rise in the number of bond configurations and thus of entropy. But bonded and normal HDL structures have the same symmetry, so that the density of the bonded structure eventually becomes equal to that of the normal structure, as temperature rises, and the TMD line may be considered as the midpoint of a continuous change between the two structures, in the same liquid phase.

The effect of pressure on the bonded HDL structure can be deduced by noting that pressure itself contributes to decrease the molecular volume. Thus, at higher pressures (but still below $p=1$) the change from the bonded to the normal structure is more favorable, and the position of the TMD line is shifted to lower temperatures, tending toward $t=0$ at $p=1$. The structural parameters of the liquid are also affected, and the absolute rates of variation in density, entropy, and number of hydrogen bonds are significantly increased as $p=1$ is approached from below (see Fig. 7). In the case of the normal HDL liquid, the role of pressure is the opposite of the former, yielding smaller absolute rates of variation of those quantities.

Comparison of the BEG and BL models [Fig. 7(a) and 7(b)] shows that the BEG model presents a smoother density variation, accompanied by less abrupt variations in $\Delta\rho_f$, as compared to ρ_{hb} of the BL model. Entropy, on the other hand, presents higher rates of variation for the BEG model. These features are related to the fact that, for a pair of neighboring molecules, there are more states compatible with a $\Delta\rho_f$ coupling than with a hydrogen bond. Because of this "flexibility" of the BEG model, a lower density increase is enough to maximize the entropy on the network of $\Delta\rho_f$ couplings. For the same reason, $\Delta\rho_f$ tends to a limiting value, at higher temperatures, which is larger than the limiting value for ρ_{hb}.

Our data for the model susceptibilities can also be discussed in terms of the competition between two structures. Figures 8(a) and 8(b) display isothermal compressibilities in accordance with the criterion put forward by Sastry *et al.* [13], which states that the presence of a negatively inclined TMD line implies decreasing isothermal compressibility, at the same pressure. The maxima in k_t are displaced toward smaller temperatures with increasing heights in the neighborhood of $p=1$. The same behavior is observed in c_p. The maxima observed on these two functions are related to large fluctuations in the molecular volume and in entropy, and are consistent with the competition between two structured liquids in the same thermodynamic phase. Although these fluctuations in volume and entropy are increasing while approaching $p=1$ at $t=0$, they are not related to a second critical point because the isovolumetric specific heat, which is proportional to fluctuations in energy, does not increase in the same region, as shown in Figs. 8(e) and 8(f)

C. Frustration

The importance of frustration in the BL model is easily recognizable when the Hamiltonian is written in a spin-1

representation, as in Eq. (7), since the linear spin coupling is seen to be antiferromagnetic.

It is usually accepted that the prototype of an energetically frustrated system is the antiferromagnetic Ising model on the triangular lattice. This model has been studied at zero magnetic field by Wannier [61], who found a paramagnetic phase at all temperatures, without any phase transition at finite temperatures. In addition, Wannier's solution predicts a residual entropy at null temperature. Both the BL and the antiferromagnetic BEG models are reduced to the antiferromagnetic Ising model in the infinite-pressure limit, when the lattice becomes completely filled. This is readly seen from Eq. (7): except for the linear spin coupling, the other terms of the Hamiltonian become configuration independent for density $\rho=1$. Our results are consistent with Wannier's predictions, since at very high pressures both models presents a residual entropy in the ground state of the HDL phase [see Figs. 7(e) and 7(f)], and no phase transition at finite temperature.

We propose an extension of the application of the concept of frustration associated with the antiferromagnetic spin-1/2 Ising model on the triangular lattice to spin-1 systems such as the ones treated in this study. For the BL model, the main effect of frustration is that it provides a natural restriction for the formation of a complete hydrogen-bonded network of molecules on the full lattice (or, analogously, of an antiferromagnetically coupled net of integer spins, in the BEG model). Considering the frustrated interactions to be "stronger" than the unfrustrated van der Waals interactions [i.e., that inequality (34) is satisfied], the appearance of a bonded structure of lower density $\rho<1$ at lower pressures is to be expected. The density anomaly which arises from the competition between the bonded and normal liquids may thus be assigned to frustration.

In order to further develop our ideas on the possible role of frustration, let us consider a different orientational lattice gas model (OLG) analyzed previously by one of us [39]. In the OLG model, molecules with four bonding and two inert arms sit on a triangular lattice. Energetic ingredients include hydrogen bonds and isotropic van der Waals interactions. Fully bonded nets are possible for a low-density state, as well as for the high-density state, and the model may thus be considered unfrustrated. However, the LDL phase is stable only if the "van der Waals" interaction is repulsive. Only in this case does the model present a liquid-liquid phase transition and a TMD line. It must be noted, however, that, unlike the BL model, the OLG model presents HDL and LDL phases of the same symmetry, with a liquid-liquid line ending in a critical point. The BL model presents two liquids with different symmetries and no critical point.

Despite the differences between the BL and the OLG models, it is possible to extend the idea of frustration to include the latter, by considering that repulsive van der Waals interactions introduce restrictions on the formation of a fully hydrogen-bonded network of molecules on the filled lattice. It would then be possible to classify all such systems as frustrated: either lattice frustrated, as would be the case of the BL and BEG models, or energetically frustrated, as in the case of the OLG model. Such a classification scheme for frustrated lattice models requires further clarification.

VI. CONCLUDING REMARKS

The Bell-Lavis model for liquid water has been compared to its isotropic version: the antiferromagnetic Blume-Emery-Griffiths model on the triangular lattice. The ground state phase diagrams of the two models were shown to be topologically identical, with fluid phases (gas and low- and high-density liquids) being equivalent to magnetic phases (paramagnet, antiferromagnet, and frustrated paramagnet). Finite-temperature effects have been considered by studying the system in the interior of the sequential Husimi cactus. Phase diagrams and maximum density lines in the high-density liquid phase were compared for equivalent values of the reduced interaction strength in both models. The anomalous features of the high-density liquid were shown to be very similar, with lines of maximum density occurring at equivalent pressures and temperatures. The stability of the LDL is substantially enhanced in the BL model, as compared to the BEG model. The larger LDL phase drives the anomalous behavior into a metastable regime of the HDL phase. For the isotropic BEG model, the line of maximum density, followed by anomalous response functions, occurs in the stable regime. The presence of these features in the BEG model shows that the orientational character of the hydrogen bond is unimportant for the anomalous behavior presented by the BL model, as observed in previous studies of continuous core-softened models [19,62,63].

In both models, the density anomaly is accompanied by a large rate of variation in entropy and number of (generalized) hydrogen bonds per particle, and by anomalous behavior of the thermodynamical response functions.

We propose to explain the anomalous behavior presented by both models through a competition between two structured liquids. We suggest that this competition would arise due to energetic frustration related to restrictions imposed on the maximum number of bonds per triangle. We also propose that energetic frustration, as a natural restriction for the formation of favorable interactions, may be responsible for anomalous liquid properties on lattices. Further studies on different models and lattices (specially in three dimensions) are being planned to test the possible relation between frustration, density anomaly, and liquid-liquid phase transitions.

ACKNOWLEDGMENTS

We would like to thank S. Salinas, M. J. de Oliveira, J. Stilck, B. Widom, B. W. Southern, and D. A. Lavis for useful discussions and suggestions. M.A.A.B. acknowledges hospitality from R. Gargano and A. F. Pereira de Araujo, and the computational support from LCCC, during a visit to Universidade de Brasília. This work has been supported by FAPESP.

[1] C. A. Angell and H. Kanno, Science **193**, 1121 (1976).
[2] D. Eisenberg and W. Kauzmann, *The Structure and Properties of Water* (Clarendon Press, Oxford, 1969).
[3] P. G. Debenedetti, *Metastable Liquids: Concepts and Principles* (Princeton University Press, Princeton, NJ, 1996).
[4] P. G. Debenedetti, J. Phys.: Condens. Matter **15**, R1669 (2003).
[5] R. J. Speedy, J. Phys. Chem. **86**, 982 (1982).
[6] P. H. Poole, F. Sciortino, U. Essmann, and H. E. Stanley, Nature (London) **360**, 324 (1992).
[7] D. J. Lacks, Phys. Rev. Lett. **84**, 4629 (2000).
[8] Y. Katayama, T. Mizutani, W. Utsumi, O. Shimomura, M. Yamakata, and K. Funakoshi, Nature (London) **403**, 170 (2000).
[9] G. Monaco, S. Falconi, W. A. Crichton, and M. Mezouar, Phys. Rev. Lett. **90**, 255701 (2003).
[10] O. Mishima and H. E. Stanley, Nature (London) **392**, 164 (1998).
[11] O. Mishima and H. E. Stanley, Nature (London) **396**, 329 (1998).
[12] T. Loerting and N. Giovambattista, J. Phys.: Condens. Matter **18**, R919 (2006).
[13] S. Sastry, P. G. Debenedetti, F. Sciortino, and H. E. Stanley, Phys. Rev. E **53**, 6144 (1996).
[14] L. P. N. Rebelo, P. G. Debenedetti, and S. Sastry, J. Chem. Phys. **109**, 626 (1998).
[15] I. Saika-Voivod, F. Sciortino, T. Grande, and P. Poole, Philos. Trans. R. Soc. London, Ser. A **363**, 525 (2005).
[16] M. R. Sadr-Lahijany, A. Scala, S. V. Buldyrev, and H. E. Stanley, Phys. Rev. E **60**, 6714 (1999).
[17] A. Scala, M. R. Sadr-Lahijany, N. Giovambattista, S. V. Buldyrev, and H. E. Stanley, Phys. Rev. E **63**, 041202 (2001).
[18] E. A. Jagla, Phys. Rev. E **58**, 1478 (1998).
[19] E. A. Jagla, J. Chem. Phys. **111**, 8980 (1999).
[20] E. A. Jagla, Braz. J. Phys. **34**, 17 (2004).
[21] G. Franzese, G. Malescio, S. V. B. Anna Skibinsky, and H. E. Stanley, Nature (London) **409**, 692 (2001).
[22] G. Franzese, J. Mol. Liq. **136**, 267 (2007).
[23] A. B. Oliveira, G. Franzese, P. A. Netz, and M. C. Barbosa, J. Chem. Phys. **128**, 064901 (2008).
[24] H. M. Gibson and N. B. Wilding, Phys. Rev. E **73**, 061507 (2006).
[25] E. Lomba, N. G. Almarza, C. Martin, and C. McBride, J. Chem. Phys. **126**, 244510 (2007).
[26] G. M. Bell, J. Math. Phys. **10**, 1753 (1969).
[27] A. B. de Oliveira and M. C. Barbosa, J. Phys.: Condens. Matter **17**, 399 (2005).
[28] K. A. T. Silverstein, A. D. J. Haymet, and K. A. Dill, J. Am. Chem. Soc. **120**, 3166 (1998).
[29] T. M. Truskett and K. A. Dill, J. Chem. Phys. **117**, 5101 (2002).
[30] T. M. Truskett and K. A. Dill, J. Phys. Chem. B **106**, 11829 (2002).
[31] F. L. Somer and J. Kovac, J. Chem. Phys. **102**, 8995 (1995).
[32] K. A. T. Silverstein, A. D. J. Haymet, and K. A. Dill, J. Chem. Phys. **111**, 8000 (1999).
[33] G. M. Bell and D. A. Lavis, J. Phys. A **3**, 568 (1970).
[34] D. A. Lavis, J. Phys. C **6**, 1530 (1973).
[35] A. P. Young and D. A. Lavis, J. Phys. A **12**, 229 (1979).
[36] B. W. Southern and D. A. Lavis, J. Phys. A **13**, 251 (1980).
[37] C. J. Roberts and P. G. Debenedetti, J. Chem. Phys. **105**, 658 (1996).
[38] C. J. Roberts, A. Z. Panagiotopoulos, and P. G. Debenedetti, Phys. Rev. Lett. **77**, 4386 (1996).
[39] V. B. Henriques and M. C. Barbosa, Phys. Rev. E **71**, 031504 (2005).
[40] V. B. Henriques, N. Guisoni, M. A. Barbosa, M. Thielo, and M. Barbosa, Mol. Phys. **103**, 3001 (2005).
[41] M. Girardi, A. L. Balladares, V. B. Henriques, and M. Barbosa, J. Chem. Phys. **126**, 064503 (2007).
[42] G. M. Bell, J. Phys. C **5**, 889 (1972).
[43] G. M. Bell and D. W. Salt, J. Chem. Soc., Faraday Trans. 2 **72**, 76 (1976).
[44] M. Pretti and C. Buzano, J. Chem. Phys. **121**, 11856 (2004).
[45] C. Buzano, E. D. Stefanis, A. Pelizzola, and M. Pretti, Phys. Rev. E **69**, 061502 (2004).
[46] N. A. M. Besseling and J. Lyklema, J. Phys. Chem. **98**, 11610 (1994).
[47] S. Sastry, F. Sciortino, and H. E. Stanley, J. Chem. Phys. **98**, 9863 (1993).
[48] D. A. Lavis, J. Phys. A **8**, 1933 (1975).
[49] G. Grigelionis and A. Rosengren, Physica A **208**, 287 (1994).
[50] P. D. Gujrati, Phys. Rev. Lett. **74**, 809 (1995).
[51] J. L. Monroe, Physica A **256**, 217 (1998).
[52] M. Pretti, J. Stat. Phys. **111**, 993 (2003).
[53] D. Tabor, *Gases, Liquids and Solids* (Cambridge University Press, Cambridge, U.K., 1991).
[54] It must be remembered that the interpolating Hamiltonian used in this work is a matter of choice. It would be possible, for instance, to interpolate between the BEG and BL Hamiltonians by considering an extended hydrogen bond interaction of the kind $g_{\mathrm{hb}}=-\epsilon_{\mathrm{hb}}[P_{\mathrm{LDL}}(S_a,S_b,S_c)+(1-\lambda)P_{\mathrm{ULDL}}(S_a,S_b,S_c)]$, with P_{LDL} and P_{ULDL} being the probability of finding the triangle's configuration in a low-density liquid state and in an unbonded low-density liquid state, described in Table I.
[55] A. Pelizzola and M. Pretti, Phys. Rev. B **60**, 10134 (1999).
[56] A. Patrykiejew, O. Pizio, and S. Sokolowski, Phys. Rev. Lett. **83**, 3442 (1999).
[57] G. Jaeger, Arch. Hist. Exact Sci. **53**, 51 (1998).
[58] Z. F. Wang, B. W. Southern, and D. A. Lavis, Phys. Rev. B **67**, 054415 (2003).
[59] B. W. Southern and D. A. Lavis (private communication).
[60] S. Bekhechi, B. W. Southern, A. Peles, and D. Mouhanna, Phys. Rev. E **74**, 016109 (2006).
[61] G. H. Wannier, Phys. Rev. **79**, 357 (1950).
[62] A. B. Oliveira, P. A. Netz, T. Colla, and M. C. Barbosa, J. Chem. Phys. **124**, 084505 (2006).
[63] A. B. Oliveira, P. A. Netz, T. Colla, and M. C. Barbosa, J. Chem. Phys. **125**, 124503 (2006).